arXiv:1406.0417v2 [gr-qc] 10 Mar 2015

Equilibrium configuration of perfect fluid orbiting around black holes in some classes of alternative gravity theories

Sumanta Chakraborty

IUCAA, Post Bag 4, Ganeshkhind, Pune University Campus, Pune 411 007, India

E-mail: sumantac.physics@gmail.com; sumanta@iucaa.ernet.in

Abstract. The hydrodynamic behaviour of perfect fluid orbiting around black holes in spherically symmetric spacetime for various alternative gravity theories has been investigated. For this purpose we have assumed an uniform distribution for the angular momentum density of the rotating perfect fluid. The contours of equipotential surfaces are illustrated in order to obtain the nature of inflow and outflow of matters. It has been noticed that, the marginally stable circular orbits originating from decreasing angular momentum density lead to closed equipotential surfaces along with cusp allowing existence of accretion disks. On the other hand, the growing part of angular momentum density exhibits central rings for which stable configurations are possible. However inflow of matter is prohibited. Among the solutions discussed in this work, the charged $F(R)$ gravity and Einstein-Maxwell-Gauss-Bonnet solution exhibit inflow and outflow of matter with central rings present. These varied accretion disk structure of perfect fluid attribute these spacetimes astrophysical importance. The effect of higher curvature terms predominantly arises from region near the black hole horizon. Hence the structural difference of accretion disk in modified gravity theories with comparison to general relativity may act as an experimental probe for these alternative gravity theories.

1. Introduction

General Relativity (GR) is a very successful theory and is the best contender, so far to describe the geometrical properties of the spacetime. It has passed through all the experimental and observational tests so far, ranging from local gravity tests like perihelion precession and bending of light to precision tests using pulsars [1, 2, 3, 4, 5]. In spite of these outstanding success for GR there are still unresolved issues. These include: the problem of Dark energy and the problem of inflation. Phrased in a different way, the reason for accelerated expansion of the universe at both very small scale and very large scale is unknown [6, 7, 8]. These issues are generally dealt with by assuming existence of additional matter component in the universe, like cosmological constant, fluid with complicated equation of state, scalar fields etc. However all these models are plagued with several issues, e.g., coupling with usual matter, consistency with elementary particle theories and consistency of formulation [9, 10, 11]. These results prompted research in a new direction by modifying the Einstein-Hilbert (EH) action for GR itself.

This idea of modifying the EH action stem from the belief that GR is just a low energy approximation of some underlying fundamental theory [12, 13]. In this spirit the classical generalizations of EH action should explain both early-time inflation and late-time cosmic acceleration without ever introducing additional matter components in the energy momentum tensor. There exist large number of ways in which the standard EH action can be modified by introducing non-linear terms. However the criteria that the field equations should remain second order in the dynamical variable (otherwise some ghost fields would appear) uniquely fixes the action to be the Lanczos-Lovelock action [14, 15, 16]. The Lanczos-Lovelock Lagrangian has this special property that though the Lagrangian contains higher curvature terms the field equation turns out to be of second order [17, 18]. One of the important model is the second order correction term in the gravity action in addition to EH term, called Gauss-Bonnet (GB) Lagrangian.

Another such model explaining the above mentioned problems is obtained by replacing R, the scalar curvature in the EH action by some arbitrary function of the scalar curvature $F(R)$. This alternative theory for describing gravitational interaction is very interesting in its on right, for it can provide an explanation to a large number of experimental phenomenon. These include: late time cosmic acceleration [19], early power law inflation [20], problem of singularity in strong gravity regime [21] along with possible detection of gravitational waves [22]. Compatibility with Newtonian and post-Newtonian approximations as well as estimations of cosmological parameters are shown in [8, 23]. $F(R)$ theories can also bypass a long known instability problem, called 'Ostrogradski' instability [24] and is capable of explaining recent graviton mass bound in LHC, with possible constraints on the model itself [25].

There also exist quiet a few gravity models, which comes into existence from some low energy string inspired theories. For example the GB Lagrangian discussed earlier is actually a low energy realization of a string inspired model [26]. In this context, we should mention that there exist a natural generalization of the Reissner-Nordström (RN)

solution in GR to that in string inspired models with dilaton coupling. The dilaton field couples with the electromagnetic field tensor $F_{\mu\nu}$ in such a fashion that every solution with non-zero $F_{\mu\nu}$ couples with the dilaton field [27, 28, 29, 30].

In this work our main aim is to obtain the equilibrium configuration of perfect fluid rotating around black holes in these alternative gravity theories. This in turn will allow us to address the new features that come out in comparison to their general relativistic counterpart. For this purpose we have first studied the equilibrium configuration of fluid in a general static spherically symmetric spacetime. Having derived various quantities of interest in this general context, we apply them to the black hole solutions in various alternative gravity theories. This can be achieved by substituting the metric elements describing spherically symmetric spacetime in these alternative theories into our general result. Throughout this work we have mainly concentrated on three alternative theories, the $F(R)$ gravity theory, dilaton induced gravity theory and finally the Einstein-Maxwell-Gauss-Bonnet (EMGB) gravity.

After deriving the results for a general static spherically symmetric spacetime, as a warm up we have applied our results to the RN solution in Einstein gravity. Then we have applied these results to a charged black hole solution in $F(R)$ gravity theory. It turns out that the equipotential contours of the perfect fluid rotating around black hole in this gravity model are quiet different from its GR counterpart. Identical features are shared by the equilibrium configuration of perfect fluid rotating around black hole in the EMGB theory as well. However the equipotential contours of perfect fluid rotating around black holes in dilaton gravity are different from the previous two situations. Still the equipotential contours exhibit features distinct in comparison to the respective GR solution. All these results suggest that the equilibrium configurations of perfect fluid rotating around black holes in alternative gravity theories have structures different from GR. By comparing these alternative theories under one roof, as presented in this work, we have been able to understand the structure of accretion disks and in-fall of matter to them in some detail. This might help to understand the accretion disk structure around other black hole solutions by direct comparison with results presented in this work.

Since the accretion disk is intimately connected with various astrophysical processes, it is natural to ask for some observational consequences of our result. We should stress at this point that though the accretion disk structure gets modified with outflow and inflow of matter associated due to introduction of alternative theories it is unlikely to be observed in an observational test. These results have to do with the fact that the accretion disk structure across a black hole in these alternative theories are determined by the dimensionless parameter $y = \Lambda M^2/12$ in geometrized units, where Λ is the cosmological constant and M being the black hole mass. In order to have stable circular orbits necessary for existence of accretion disc, the cosmological parameter has a restriction $y < y_e \sim 4.8 \times 10^{-5}$ as we have shown later. Along with we can use cosmological tests using magnitude-redshift relation for supernova with the measurements of Cosmic Microwave Background (CMB) fluctuation [42, 43] implying $\Lambda \sim 10^{-56}$ cm^{-2}. This leads to very low values of y for realistic black holes. For

example, in case of an extremely massive black hole as seen in quasar TON 618, with mass $\sim 6.6 \times 10^{10} M_{\odot}$ [44] leads to $y \sim 4.1 \times 10^{-25}$. This suggests that the parameter space for observations in astrophysical scenarios has the value of cosmological parameter $y \sim 10^{-30}$. This is quiet small compared to the value $y \sim 10^{-7}$ presented in the text for being of astrophysical importance [31, 32, 33, 34, 35, 36, 37, 38, 39]. Thus for normal astrophysical systems it is difficult to detect any departure from the result predicted by GR. Even for quiet massive systems departure from GR, with observed accuracy has not been found to date ‡. Such small values are out of the parameter space for present day astrophysical observations, making the test for these alternative theories difficult.

However there is another window to look for signatures of these alternative theories. For primordial black holes in the early universe the *effective* cosmological constant was higher [45] and consequently y would had a much larger value of comparable to y_e. Thus in the early universe the accretion disk structure around primordial black holes may posses the features discussed in this work. But this is also far from being observed experimentally. In spite of these difficulties in relating to observational results, the work stands on its own, for it describes the accretion structure in alternative theories and its departure from the GR results. For some choice of the parameter space the structure in alternative theories are much rich and differ significantly from that in GR. This analysis brings out the fact that introduction of higher curvature terms in the EH action alters the accretion disk structure of perfect fluid orbiting the black hole in a non-trivial manner with more structures included.

The paper is organized as follows: In section 2 we have illustrated the Boyer's condition [46, 47, 48] in order to have an equilibrium configuration of the perfect fluid. Then in the next section 3 we have derived various physical quantities for a general static spherically symmetric spacetime, which we have subsequently applied to determine equipotential surfaces of fluid moving around various black hole solutions in different gravity theories. Among these alternative theories we have discussed the RN solution, topologically charged black hole in $F(R)$ theory, charged black hole in dilaton gravity and finally black hole in EMGB theory in 4. At the end we conclude with a discussion on our results.

2. Equilibrium configuration of rotating perfect fluid

In this section we briefly summarize the well known results regarding general theory of equipotential surfaces inside any relativistic, differentially rotating, perfect fluid body [46, 47]. This has also been applied to configurations of perfect fluid rotating in the stationary and axi-symmetric spacetimes [35, 36, 37]. In standard coordinate system

‡ one such system where the effect can be observed is a pulsar-White Dwarf (WD) system. Such a recent system, PSR J0348+0432 has a huge mass for the Neutron star, making sensitive test for the strong gravity regime possible. To date the orbital period decay of this system is in agreement with GR [40]. Another such system PSR J1738+0333 also shows results consistent with GR [41].

the spacetime is described by the following line element,

$$ds^2 = g_{tt}dt^2 + 2g_{t\phi}dtd\phi + g_{\phi\phi}d\phi^2 + g_{rr}dr^2 + g_{\theta\theta}d\theta^2 \tag{1}$$

where the metric elements depend neither on time coordinate t nor on azimuthal coordinate ϕ. Hence energy and angular momenta are two conserved quantities in this spacetime implying existence of two killing vectors $\frac{\partial}{\partial t}$ and $\frac{\partial}{\partial \phi}$. We shall consider perfect fluid rotating in the ϕ direction. Then its four velocity field U^μ has only two non-zero components,

$$U^\mu = \left(U^t, U^\phi, 0, 0\right) \tag{2}$$

which can be functions of the coordinates (r, θ). The stress energy tensor of the perfect fluid is,

$$T^\mu_\nu = (p + \epsilon)U^\mu U_\nu + p\delta^\mu_\nu \tag{3}$$

where ϵ and p denote the total energy density and the pressure of the fluid. The rotating fluid can be characterized by the vector fields of the angular velocity Ω, and the angular momentum per unit mass (angular momentum density) ℓ, defined by

$$\Omega = \frac{U^\phi}{U^t}; \qquad \ell = -\frac{U_\phi}{U_t} \tag{4}$$

These vector fields are related to the metric elements by the following result

$$\Omega = -\frac{g_{t\phi} + \ell g_{tt}}{g_{\phi\phi} + \ell g_{t\phi}} \tag{5}$$

In static spacetimes ($g_{t\phi} = 0$), the above relation reduces to the simple formula

$$\frac{\Omega}{\ell} = -\frac{g_{tt}}{g_{\phi\phi}} \tag{6}$$

The surfaces of constant ℓ and Ω are called von Zeipel's cylinders. These surfaces do not depend on the rotation law for fluids in static spacetimes but do depend on the rotation law for stationary spacetimes [35].

Projecting the stress energy tensor conservation law $\nabla_\nu T^{\mu\nu} = 0$ onto the hypersurface orthogonal to the four velocity U^μ by the projective tensor $h_{\mu\nu} = g_{\mu\nu} + U_\mu U_\nu$, we obtain the relativistic Euler equation in the form,

$$\frac{\partial_\mu p}{p + \epsilon} = -\partial_\mu(\ln U_t) + \frac{\Omega\partial_\mu \ell}{1 - \Omega\ell} \tag{7}$$

where

$$(U_t)^2 = \frac{g^2_{t\phi} - g_{tt}g_{\phi\phi}}{g_{\phi\phi} + 2\ell g_{t\phi} + \ell^2 g_{tt}} \tag{8}$$

The solution to the relativistic Euler equation given in Eq. (7) can be obtained by defining the potential $W(r, \theta)$ whose "equipotential surfaces" are surfaces of constant pressure through the following relation [36, 48, 49]:

$$\int_0^p \frac{dp}{p + \epsilon} = W_{in} - W \tag{9}$$

which leads to

$$W_{in} - W = ln(U_t)_{in} - ln(U_t) + \int_{\ell_{in}}^{\ell} \frac{\Omega d\ell}{1 - \Omega\ell} \tag{10}$$

The subscript "in" in the above equations refer to the inner edge of the disk. For an alternative definition and thus derivation of Boyer's conditions see Ref. [36, 50, 51]. The equipotential surfaces are determined by the condition, $W(r, \theta) =$ constant and in a given spacetime W can be found from Eq. (10), if the rotation law $\Omega = \Omega(\ell)$ is known. The surfaces of constant pressure are being determined by Eq. (9). The structure of thick accretion disks can also be found using the accurate Newtonian framework called Pseudo-Newtonian Potential method [52, 53].

3. Equilibrium configuration of a Perfect Fluid for a general spherically symmetric spacetime

In this section we shall start with a general metric ansatz. This is very appropriate for describing various static spherically symmetric solutions in both Einstein gravity or other alternative gravity theories [54, 55]. The metric ansatz is simple enough that it can be easily generalized to arbitrary number of spacetime dimensions. The general metric ansatz is taken as,

$$ds^2 = -f(r)dt^2 + f(r)^{-1}dr^2 + r^2 d\Omega^2 \tag{11}$$

Note that the characteristic property of equipotential surfaces is retained in this simplest choice, which is uniform distribution of angular momentum density ℓ [37]. The importance of the above statement enhances considerably from the fact that marginally stable configurations comes into existence under the condition [56]

$$\ell(r, \theta) = \text{const} \tag{12}$$

This holds for any rotating fluid irrespective of its rotation law for static spacetime (however for stationary spacetime the above condition depends on the rotation law [35]). Using which we can obtain the following expression for equipotential surfaces from Eq. (10) as

$$W(r, \theta) = \ln U_t(r, \theta) \tag{13}$$

Note that the quantity $U_t(r, \theta)$ depends only on the metric and is being completely determined by Eq. (12). The equation for these equipotential surfaces are to be given by the following relation $\theta = \theta(r)$, which can be obtained by solving the following differential equation

$$\frac{d\theta}{dr} = -\frac{\partial p/\partial r}{\partial p/\partial \theta} \tag{14}$$

For the $\ell =$ constant configurations the above expression leads to,

$$\frac{d\theta}{dr} = -\frac{\partial U_t/\partial r}{\partial U_t/\partial \theta} \tag{15}$$

Having obtained all these basic tools we now proceed to determine the equilibrium configuration of perfect fluid orbiting around a black hole in a spacetime with a metric ansatz given by Eq. (11). Thus the potential turns out to be

$$W(r,\theta) = \ln\left[\frac{r\sin\theta\sqrt{f(r)}}{\sqrt{r^2\sin^2\theta - \ell^2 f(r)}}\right] \tag{16}$$

as well as the differential equation satisfied by θ leads to

$$\frac{d\theta}{dr} = \frac{r^3\sin^2\theta f'(r) - 2\ell^2 f(r)^2}{2r\ell^2 f(r)^2}\tan\theta \tag{17}$$

where 'prime' denotes derivative with respect to the radial co-ordinate r. The insight about the ℓ = constant surfaces are gained by examination of the potential $W(r,\theta)$ in the equatorial plane $\theta = \pi/2$. From physical principles the potential should be real and that eventually leads to the following conditions

$$f(r) \geq 0 \tag{18}$$

$$r^2 - \ell^2 f(r) \geq 0 \tag{19}$$

The first condition would lead to static regions outside the black hole horizon where the perfect fluid orbiting the black hole can have equilibrium configurations. The second condition can be expressed in an elegant form as:

$$\ell^2 \leq \ell^2_{ph} \equiv \frac{r^2}{f(r)} \tag{20}$$

where the function defined as ℓ^2_{ph} is the effective potential of photon geodesic, with impact parameter $\ell = U_\phi/U_t$ [57]. Note that the extremization of the potential $W(r,\theta=\pi/2)$ being identical with the condition that pressure gradient should vanish i.e. $\partial U_t/\partial r = 0$ and $\partial U_t/\partial\theta = 0$. However since we are concerned with the equatorial plane ($\theta = \pi/2$), the criteria $(\partial W/\partial r) = 0$ is sufficient for maximization of $W(r,\theta=\pi/2)$ leading to

$$\frac{\partial U_t(r,\theta=\pi/2)}{\partial r} = \frac{r^3 f'(r) - 2\ell^2 f(r)^2}{2\sqrt{f}\left[r^2 - \ell^2 f(r)\right]^{3/2}} \tag{21}$$

It is well known that the extrema of the potential on the equatorial plane $W(r,\theta = \pi/2)$ corresponds to motion along circular geodesics. Thus the angular momentum distribution ℓ^2_K obtained from the condition $\partial_r U_t = 0$ represents the angular momentum density for circular orbits. From Eq. (21) the following estimation of angular momentum density ℓ^2_K becomes possible

$$\ell^2_K = \frac{r^3 f'(r)}{2f(r)^2} \tag{22}$$

With this identification of ℓ^2_K, the extrema for the potential $W(r,\theta = \pi/2)$ can be obtained as

$$W_{extrema}(r,\theta=\pi/2) = \ln E_c \tag{23}$$

which determines

$$E_c(r) = \frac{\sqrt{2}f(r)}{\sqrt{2f(r) - rf'(r)}} \tag{24}$$

to be the specific energy attributed for motion along circular geodesics. Thus in order to summarize our results, we have discussed that one of the most important properties of the potential $W(r,\theta)$ is that its behaviour at equatorial plane $\theta = \pi/2$ completely determines all the parameters under interest through ℓ^2_{ph} and ℓ^2_K. From these two angular momentum densities we will be able to introduce more parameters in order to explain the behaviour of the fluid configuration in an compact and understandable fashion.

For that purpose there exists two equations of utmost importance. One of them comes from the fact that minima of ℓ^2_{ph} gives the photon radius r_{ph} and is determined by solving the equation,

$$rf'(r) = 2f(r) \tag{25}$$

Also note that ℓ^2_K diverges at the horizon given by $f(r) = 0$. Since we have,

$$\frac{\partial \ell^2_K}{\partial r} = \frac{2f(r)^2\left[3r^2f'(r) + r^3f''(r)\right] - 4r^3f(r)f'(r)^2}{4f(r)^4} \tag{26}$$

the local extrema of the angular momentum density ℓ^2_K is being determined by the following equation,

$$4r^3f'(r)^2 = 2f(r)\left[3r^2f'(r) + r^3f''(r)\right] \tag{27}$$

Hence all the relevant quantities necessary to uniquely characterize the fluid motion are derived for a general metric ansatz. We will henceforth use these results frequently throughout the later part of this work.

4. Equipotential Surfaces of Marginally Stable Configurations Orbiting Around Black Holes in Various Gravity Theories

In this section we will apply the results derived in the previous section to spherically symmetric and static spacetimes in both GR and alternative gravity theories. We will start with the Reissner-Nordström solution in general relativity and then subsequently will generalize to alternative gravity theories. Among these alternative theories, we will consider the black hole solution in $F(R)$ gravity first, then Einstein-Maxwell gravity with dilaton field, finally specializing to Einstein-Maxwell-Gauss-Bonnet gravity (similar aspects within GR framework has been considered in [58, 59]).

4.1. Reissner-Nordström Black Hole

Before proceeding to alternative theories we shall first consider a solution in GR itself. This will help the reader to understand various physical quantities of interest in the other theories better. The line element for the RN black hole has the following expression

$$ds^2 = -\left(1 - \frac{2M}{r} + \frac{Q^2}{r^2}\right)dt^2 + \left(1 - \frac{2M}{r} + \frac{Q^2}{r^2}\right)^{-1}dr^2 + r^2d\Omega^2 \tag{28}$$

where Q is the charge of the black hole and M is its mass. The potential $W(r,\theta)$, introduced by Eq. (9) and Eq. (16) for the above metric takes the following form

$$W(r,\theta) = \frac{1}{2}\ln\left[\frac{r^2\sin^2\theta\,(r^2-2Mr+Q^2)}{r^4\sin^2\theta-(r^2-2Mr+Q^2)\,\ell^2}\right] \tag{29}$$

Hence from the reality criteria of the potential we arrive at the following constraints

$$\left(1-\frac{2M}{r}+\frac{Q^2}{r^2}\right)\geq 0 \tag{30}$$

$$\ell^2 \leq \ell^2_{ph} = \frac{r^4}{r^2-2Mr+Q^2} \tag{31}$$

where, ℓ_{ph} corresponds to angular momentum associated with the photon orbit. Also we have the following result for $(d\theta/dr)$ from Eq. (17) as

$$\frac{d\theta}{dr} = \frac{r^4\,(Mr-Q^2)\sin^2\theta-\ell^2\,(r^2-2Mr+Q^2)^2}{r\ell^2\,(r^2-2Mr+Q^2)^2}\tan\theta \tag{32}$$

Now there are two horizons of this space time, one is the regular event horizon located at $r=r_{eh}$ and the other horizon, known as the Cauchy horizon located at $r=r_{ch}$, have the following expressions

$$r_{eh} = M+\sqrt{M^2-Q^2} \tag{33}$$

$$r_{ch} = M-\sqrt{M^2-Q^2} \tag{34}$$

Another important radius is the photon circular orbit radius, whose location in this spacetime is given by the following expression:

$$r_{ph} = \frac{3M\pm\sqrt{9M^2-8Q^2}}{2} \tag{35}$$

The extrema of the potential $W(r,\theta)$ on the equatorial plane is being determined by an angular momentum density ℓ^2_K from Eq. (22) with the following expression

$$\ell^2_K = \frac{r^4\,(Mr-Q^2)}{(r^2-2Mr+Q^2)^2} \tag{36}$$

Then we also have the following expression for derivative of ℓ^2_K:

$$\frac{\partial\ell^2_K}{\partial r} = \frac{(r^2-2Mr+Q^2)\,(5Mr^4-4r^3Q^2)-4r^4\,(r-M)\,(rM-Q^2)}{(r^2-2r+Q^2)^3} \tag{37}$$

The minima of the photon angular momentum can be obtained by plugging in Eq. (35) into Eq. (31) which leads to:

$$\ell^2_{ph(min)} = \frac{\left(3M+\sqrt{9M^2-8Q^2}\right)^4}{8\left(3M^2-2Q^2+M\sqrt{9M^2-8Q^2}\right)} \tag{38}$$

Thus we have presented all these results for a well known solution in GR to facilitate easy comparison with other gravity theories. This also brings out the key parameters involved in these computations which would be helpful as we go along discussing various alternative gravity theories.

4.2. Charged Black Hole in $F(R)$ Gravity

In this section we will restrict ourselves to four dimensional spacetime. The action in this four dimensional spacetime with $F(R)$ gravity in presence of matter field can be presented as:

$$S = \frac{1}{16\pi}\int d^4x\sqrt{-g}\left[F(R) + \mathcal{L}_{matter}\right] \tag{39}$$

In the above expression for action $F(R)$ is an arbitrary function of the Ricci scalar R and $\mathcal{L}_{matter}$ is the Lagrangian for matter fields. Then variation of the above action with respect to the metric leads to the field equation [9, 60]:

$$R_{ab}F_R - \nabla_a\nabla_b F_R + \left(\Box F_R - \frac{1}{2}F(R)\right)g_{ab} = T^{matter}_{ab} \tag{40}$$

where R_{ab} is the Ricci tensor, $F_R \equiv dF(R)/dR$ and T^{matter}_{ab} is the standard matter stress-energy tensor, derived from the matter part of the Lagrangian $\mathcal{L}_{matter}$ as given in action (39). Also the trace of the above equation connects trace of stress-energy tensor to the scalar curvature. We are interested in determining spherically symmetric solution to the above field equation. Following the analysis presented in [61] we arrive at a charged solution in this $F(R)$ gravity models with $F(R) = R - \lambda\exp(-\xi R)$. It should be noted as emphasized in Sec. 1, that these modifications in Einstein-Hilbert action should pass all tests starting from clustering of galaxies down to solar system tests. For this special exponential correction factor it has been shown [62] that there is no contradiction with solar system tests. Also the solutions of this model are indistinguishable from the standard Einstein-Hilbert solution except for a possible change in Newton's constant [63]. The solution to the above field equation presented in Eq. (40) is topologically charged and can be presented following Eq. (11) as

$$f(r) = 1 - \frac{\Lambda}{3}r^2 - \frac{M}{r} + \frac{Q^2}{r^2} \tag{41}$$

where $\Lambda = \lambda\left[(4+2\xi R)/(8e^{\xi R})\right]$. In order for this metric ansatz to satisfy Eq. (40) we should have some constraint among the parameters appearing in our theory, which are the followings [61]:

$$1 + \frac{\lambda\xi}{\exp(\xi R)} = 0 \tag{42}$$

$$\frac{\lambda}{\exp(\xi R)} + \frac{R}{2}\left(\frac{\lambda\xi}{\exp(\xi R)} - 1\right) = 0 \tag{43}$$

This solution though looks similar to the charged black hole, its higher dimensional behaviour is different. The charge term in the above expression goes as $r^{-(d-2)}$ in d dimension, while it goes as $r^{-2(d-3)}$ in standard charged higher dimensional black hole spacetime. Therefore it is interesting to ask whether this term is originating from the scalar-tensor representation of $F(R)$ gravity. In order to obtain the representation the standard way is to start with conformal transformations on the metric elements. However in this case no new physical interpretation can be obtained except its relation to the scale of the problem [10, 61, 64].

The above result can also be interpreted in a slightly different manner, uncharged solutions in $F(R) = R + f(R)$ theory shows exact similarity with Einstein gravity in presence of a cosmological constant. Thus in those situations $f(R)$ plays the role of cosmological constant. As shown in [61] this charged solution is equivalent to Einstein gravity coupled with conformally invariant Maxwell field, such that $f(R)$ term in this situation has the role of electromagnetic field. This acts as a origin of the charge term.

Next we will consider the equilibrium configurations of perfect fluid rotating around this black hole. For notational simplicity we will assume, $M = 2$, $Q = 1$ and $y = \Lambda/3$. Then the line element for this black hole spacetime reduces to the following form

$$ds^2 = -\left(1 - yr^2 - \frac{2}{r} + \frac{1}{r^2}\right) dt^2 + \frac{dr^2}{\left(1 - yr^2 - \frac{2}{r} + \frac{1}{r^2}\right)} + r^2 d\Omega^2 \tag{44}$$

We must stress that static region exists in this spacetime with sub-critical values of cosmological parameter y as

$$y < y_c = \frac{1}{16} \tag{45}$$

Thus equilibrium configurations are possible in this spacetime provided cosmological parameter y satisfies the constraint given by Eq. (45). The equipotential surfaces are being given by

$$W(r, \theta) = \ln \left[\frac{r \sin\theta \sqrt{\left(1 - yr^2 - \frac{2}{r} + \frac{1}{r^2}\right)}}{\sqrt{r^2 \sin^2\theta - \ell^2 \left(1 - yr^2 - \frac{2}{r} + \frac{1}{r^2}\right)}} \right] \tag{46}$$

as well as we have,

$$\frac{d\theta}{dr} = \frac{(2r - 2 - 2yr^4)\sin^2\theta - 2\ell^2 \left(1 - yr^2 - \frac{2}{r} + \frac{1}{r^2}\right)^2}{2r\ell^2 \left(1 - yr^2 - \frac{2}{r} + \frac{1}{r^2}\right)^2} \tan\theta \tag{47}$$

Note that for $y = 0$ it reduces to the RN scenario discussed earlier. The best idea about nature of $\ell =$ constant surface can be extracted from behaviour of the potential $W(r, \theta)$ in equatorial plane ($\theta = \pi/2$). There we have two reality conditions imposed on the potential,

$$\left(1 - yr^2 - \frac{2}{r} + \frac{1}{r^2}\right) \geq 0 \tag{48}$$

$$\ell^2 \leq \ell^2_{ph} \equiv \frac{r^2}{\left(1 - yr^2 - \frac{2}{r} + \frac{1}{r^2}\right)} \tag{49}$$

The function ℓ_{ph} represents angular momentum of photon's orbit. Further extremizing the potential $W(r, \theta = \pi/2)$ we arrive at the particular expression for angular momentum density

$$\ell^2 = \ell^2_K(r, y) \equiv \frac{(2r - 2 - 2yr^4)}{2\left(1 - yr^2 - \frac{2}{r} + \frac{1}{r^2}\right)^2} \tag{50}$$

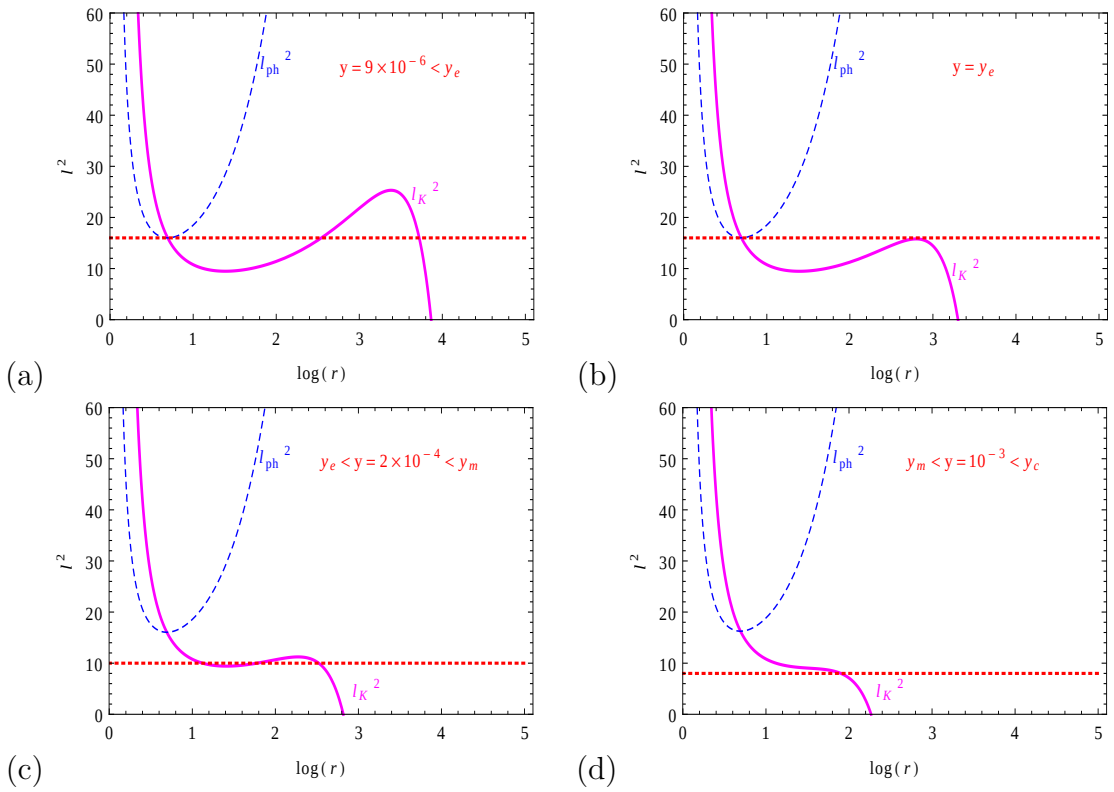

Figure 1. The figures (a)-(d) show the variation of $l^2_{ph}(r, y)$ and $l^2_K(r, y)$ with radial variable r for four different values of cosmological parameter y with $M = 2$ and $Q = 1$ (thus both ℓ^2 and r are in units of M). They reflect subsequently the following cases: (a)$0 < y < y_e$; (b)$y = y_e$; (c)$y_e < y < y_{ms}$ and (d)$y_{ms} < y < y_c$. The descending parts of ℓ^2_K determine the cusps and the growing part determines the central rings.

The specific energy of circular geodesics, corresponding to local extrema of the effective potential can be expressed as

$$E_c(r, y) = \frac{1 - yr^2 - \frac{2}{r} + \frac{1}{r^2}}{\sqrt{1 - \frac{3}{r} + \frac{2}{r^2}}} \tag{51}$$

Now we turn back to the horizons in this spacetime. For $y > 0$, the photon angular momentum $\ell^2_{ph}(r, y)$ diverges at the black hole horizon r_h and cosmological horizon r_c determined by the equality in Eq. (48). This leads to the following expression for horizons,

$$r_h = \frac{1}{2}\left(\frac{1}{\sqrt{y}} - \frac{\sqrt{1 - 4\sqrt{y}}}{\sqrt{y}}\right) \tag{52}$$

$$r_c = \frac{1}{2}\left(\frac{1}{\sqrt{y}} + \frac{\sqrt{1 - 4\sqrt{y}}}{\sqrt{y}}\right) \tag{53}$$

Also the photon circular orbit radius can be obtained from the extrema of ℓ^2_{ph}. This has the numerical value: $r_{ph} = 3.56155$. For this circular orbit the photon angular

momentum density could be given by,

$$\ell^2_{ph(c)} \equiv \ell^2_{ph}(r_{ph}, y) = \frac{12.6846}{0.359611 - 12.9846y} \tag{54}$$

Also the zero point of ℓ^2_K leads to a radius called static radius and in this black hole spacetime is expressed parametrically as,

$$y(r_s) = \frac{r_s - 1}{r_s^4} \tag{55}$$

Note that ℓ^2_K is not well defined in the region $r > r_s$, being negative there. At this static radius black hole attraction is compensated for cosmological repulsion. Then local extrema of ℓ^2_K corresponds to the following expression for cosmological parameter as,

$$y_{ms}(r) = \frac{(r-1)^4(r-4)}{r^4(12 - 15r + 4r^2)} \tag{56}$$

This determines the marginally stable circular geodesics. The local maxima of this function y_{ms} gives the critical value for the cosmological parameter y admitting stable circular orbits,

$$y_{ms} = 0.000692 \tag{57}$$

For $y < y_{ms}$, there exists an inner or outer marginally stable circular geodesic at $r_{ms(i)}$ or $r_{ms(o)}$. There exists another special value of y, which corresponds to the situation where minimum value of ℓ^2_{ph} equals the maximum of ℓ^2_K. This value is denoted by y_e and has the following numerical value,

$$y_e \sim 4.8 \times 10^{-5} \tag{58}$$

We can now separate out four different classes depending on the behavior of the functions ℓ^2_{ph} and ℓ^2_K. These four classes are defined according to the cosmological parameter in the following way,

(i) $0 < y < y_e$

(ii) $y = y_e$

(iii) $y_e < y < y_{ms}$

(iv) $y_{ms} < y < y_c$

For all these classes the variation of the two angular momentum quantities are illustrated in Fig. 1. In all these figures the descending parts of the curve $\ell^2_K(r, y)$ connects to unstable circular geodesics, along with the growing part (if exists) determining stable circular geodesics. The extrema of $\ell^2_K(r, y)$ has an important significance: the minima determines $\ell_{ms(i)}$ at $r_{ms(i)}$, the inner marginally stable circular orbit and the maxima determines $\ell_{ms(o)}$ at $r_{ms(o)}$, which corresponds to outer marginally stable circular orbit.

The equipotential surfaces are also astrophysically quiet important. Their properties can be established by studying the properties of the potential $W(r, \theta)$ in the equatorial plane. Note that the potential $W(r, \theta = \pi/2, y)$ has closely related properties

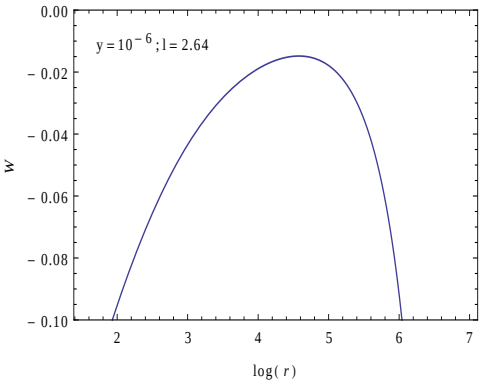

(a1)

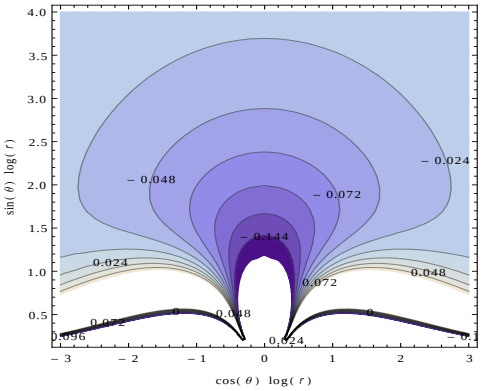

(a2)

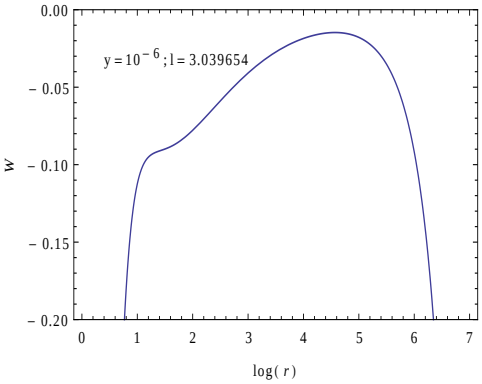

(b1)

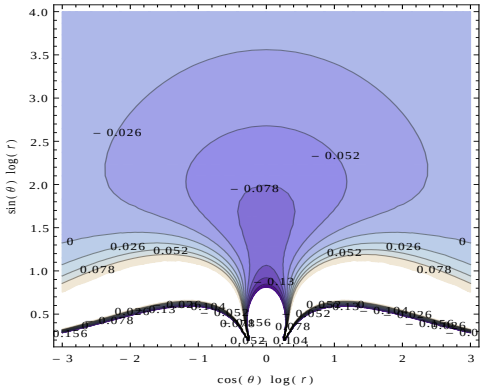

(b2)

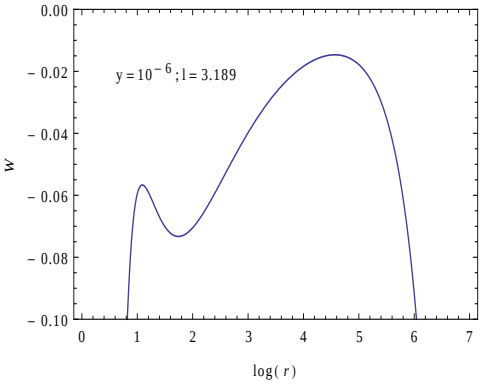

(c1)

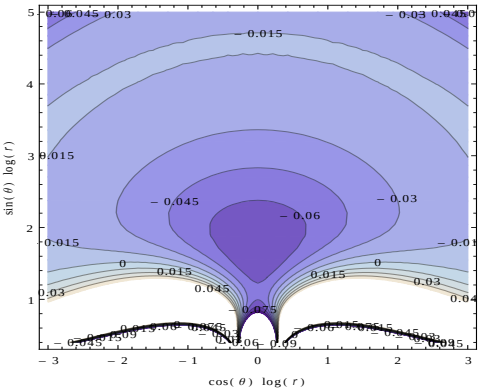

(c2)

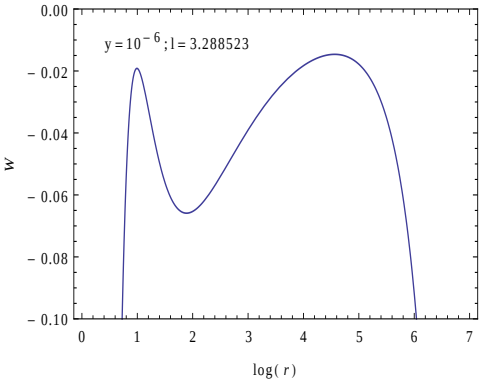

(d1)

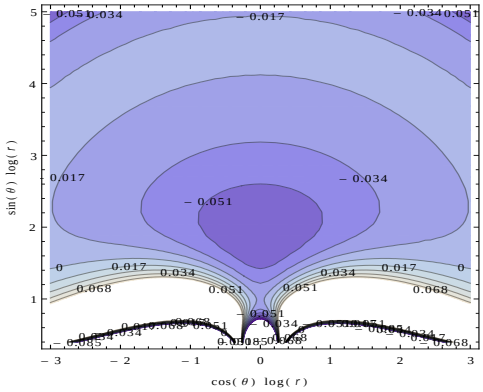

(d2)

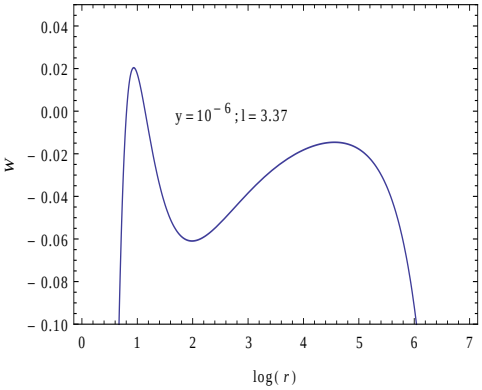

(e1)

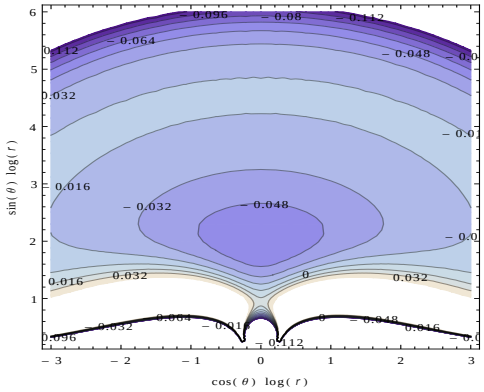

(e2)

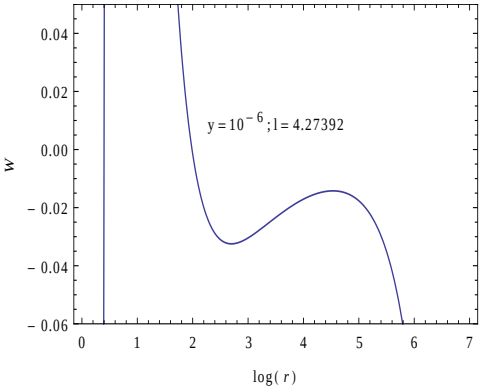

(f1)

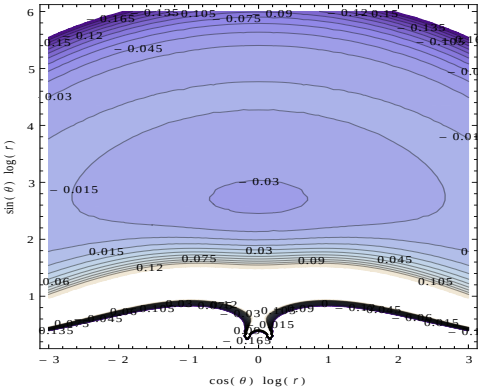

(f2)

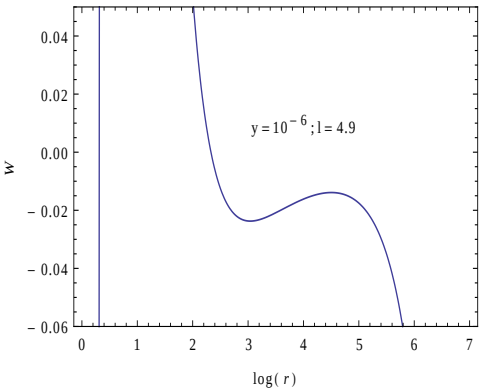

(g1)

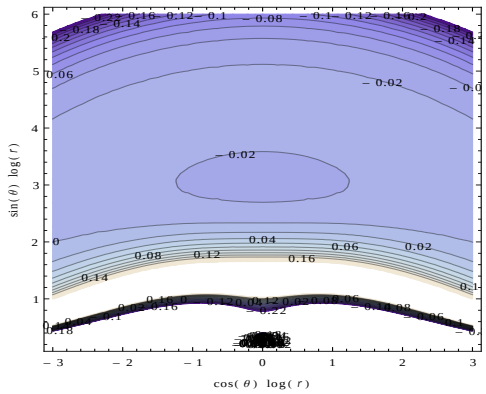

(g2)

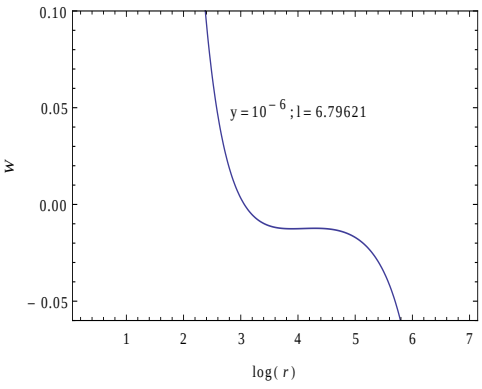

(h1)

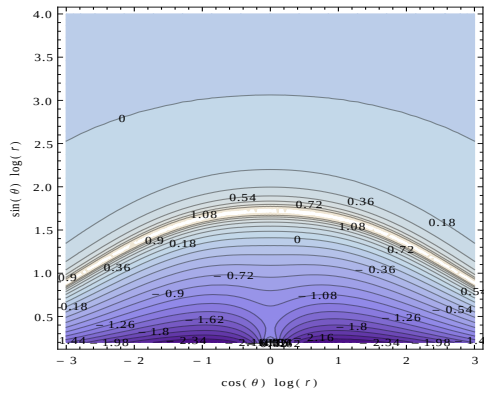

(h2)

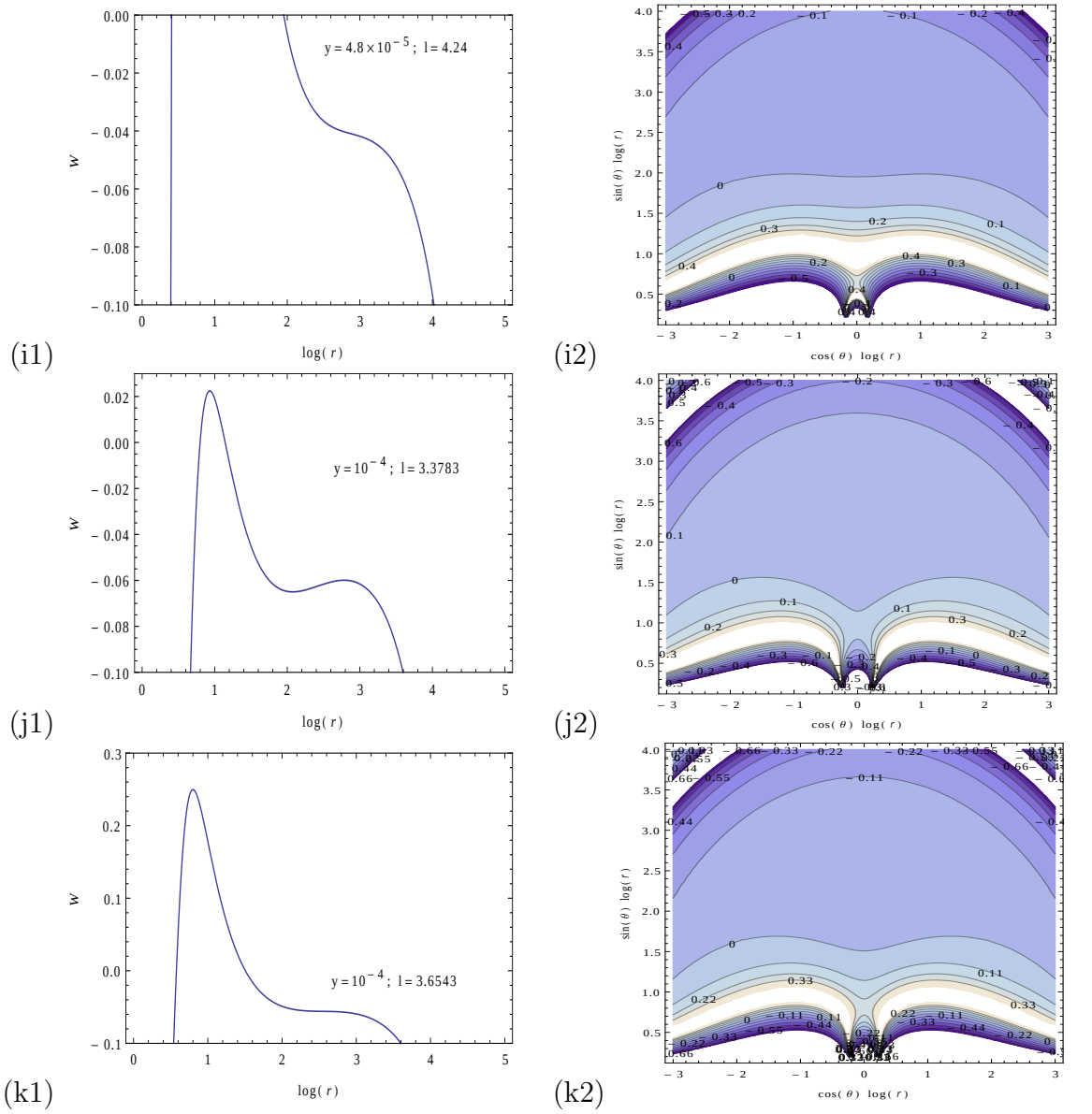

Figure 2. The figures (a)-(k) are showing the variation of potential $W(r, \theta = \pi/2, y)$ with *logr* (the '1' part) and the contour plot of W with $\log r \ \sin\theta$ and $\log r \ \cos\theta$ (the '2' part). These actually determines the equipotential surfaces i.e. meridional sections of marginally stable configurations with $\ell =$ constant for fluid motion around black hole in this $F(R)$ theory. All (a)-(k) figure shows all possible variations for different values of cosmological parameter y and angular momentum ℓ. The cusps are originating from local maxima of the potential while the central rings are from local minima. All these situations are more elaborately discussed in the text.

with effective potential of geodesic motion. It is worthwhile to mention that in the limit $r \to r_h$ or $r \to r_c$ $W(r, \theta = -\pi/2, y) \to -\infty$ hence the topological properties of the equipotential surfaces are directly inferred from the behavior of the potential $W(r, \theta = \pi/2, y)$. As pointed out earlier, local extrema of the potential is determined by the condition,

$$\ell^2 = \ell^2_K(r, y) \tag{59}$$

Hence the decreasing part of ℓ^2_K determines the maxima of the potential $W(r, \theta = \pi/2, y)$. These correspond to cusps such that at these radii matter moves along unstable geodesic orbit. While the rising part in ℓ^2_K determines the minima of the potential. These correspond to central rings of the equilibrium configurations along which matter moves in stable geodesics.

Next we provide a complete study of the behavior of equipotential surfaces along with the potential $W(r, \theta = \pi/2, y)$. We begin with the situations of astrophysical importance.

(i) $0 < y < y_e$. This is the situation illustrated in Fig.1a. Here we discuss eight different configurations according to the values of $\ell =$ constant satisfying $\ell > 0$.
   (a) $\ell < \ell_{ms(i)}$. Open surfaces are the only ones in existence, No disks are possible while surfaces with outer cusp exists (Fig. 2a1-2).
   (b) $\ell = \ell_{ms(i)}$. An infinitesimally thin, unstable ring located at $r_{ms(i)}$ exists also open surfaces with outer cusps remain in the picture (Fig. 2b1-2).
   (c) $\ell_{ms(i)} < \ell < \ell_{mb}$. Closed surfaces comes into existence. Many equilibrium configuration even without any cusp is now possible. We also have surfaces with inner and outer cusp (Fig. 2c1-2).
   (d) $\ell = \ell_{mb}$. Here also equilibrium configurations without cusps are possible. An surface come into existence with both inner and outer cusp. Also along with inflow into black hole due to mechanical non-equilibrium, an outflow from disk also occur. This comes due to the repulsive nature of the cosmological parameter. This is an astrophysically important scenario (Fig. 2d1-2).
   (e) $\ell_{mb} < \ell < \ell_{ph(c)}$. Equilibrium configurations are possible but accretion is not possible. Since we have no closed surface with inner cusp. The surface with inner cusp is an open equipotential surface, while that with outer cusp is an closed equipotential surface. This makes outflow from the disk possible (Fig. 2e1-2).
   (f) $\ell = \ell_{ph(c)}$. The potential $W(r, \theta = \pi/2, y)$ diverges at the photon circular orbit. Thus inner cusp completely disappears. Closed equipotential surfaces with outer cusp still exists enabling outflow from disk (Fig. 2f1-2).
   (g) $\ell = \ell_{ms(o)}$. An infinitesimally thin, unstable ring located at $r_{ms(o)}$ exists with coalescing outer and central cusp (Fig. 2g1-2).
   (h) $\ell > \ell_{ms(o)}$. Only open equipotential surfaces exist with no cusp. (Fig. 2h1-2)

(ii) $y = y_e$. For this special y value the variation of ℓ^2_K and ℓ^2_{ph} has been illustrated in Fig. 1b. For this case also we obtain all the hypersurfaces with similar nature. All

of them falls into a single class, given by,

(a) $\ell = \ell_{ph(c)} = \ell_{ms(o)}$. Here there exists no inner cusp only an outer cusp mixing with the center exists (Fig. 2i1-2).

(iii) $y_e < y < y_{ms}$ This situation is illustrated by Fig. 1c. However in this situation many other choices comes into existence. We classify them below,

(a) $\ell_{mb} < \ell < \ell_{ms(o)}$. This condition is equivalent to the condition (1e) illustrated above.

(b) $\ell = \ell_{ms(o)}$. This situation is slightly different. Here there exists an inner cusp of an open equipotential surface, while the outer cusp gets mixed with center corresponding to a thin ring at the radius $r_{ms(o)}$ (Fig. 2j1-2).

(c) $\ell_{ms(o)} < \ell < \ell_{ph(c)}$. This condition has only open equipotential surfaces among them one has an inner cusp (Fig. 2k1-2).

(iv) $y_{ms} < y < y_c$. For this choice of cosmological parameter the variations of ℓ_K^2 and ℓ_{ph}^2 are shown in Fig. 1d. Note that in this situation ℓ_K^2 has only a declining part. Thus we can have only maxima of the potential and existence of open equipotential surfaces. This leads to the fact that in these spacetimes stable circular geodesics do not exist. In this case there is only two physically meaningful interval.

(a) $\ell < \ell_{ph(c)}$. This situation has equipotential surfaces identical to the situation illustrated in (1a).

(b) $\ell \geq \ell_{ph(c)}$ This is similar to the situation (2a) discussed earlier.

We should also mention in this connection that the following numerical values are obtained for angular momentum densities, which are important for the study of fluid orbiting around black hole. The angular momentum density for inner marginally stable orbit is $\ell_{ms(i)} = 3.03965$, while that for outer marginally stable orbit is given by, $\ell_{ms(o)} = 4.9$ for cosmological parameter being $y = 10^{-6}$. Two other important angular momentum densities are that of marginally bound orbit with, $\ell_{mb} = 3.28852$ and for photon circular orbit as, $\ell_{ph(c)} = 4.27392$. These expressions are of quiet importance to study the structure of accretion disk.

4.3. Charged Black Hole in Dilaton Gravity

Equilibrium configurations originating from test particle fluid, which is rotating in a given spacetime are determined by the equipotential surfaces, where the gravitational and inertial forces are being compensated by the pressure gradient. (For an axially symmetric spacetime the rotation axis of the equilibrium configuration coincides with the axis of symmetry for the spacetime, while for a spherically symmetric case this axis can be any radial line; see for example [48]).

The influence of a non-zero dilaton charge coming from an effective string theory on the character of the equipotential surfaces of marginally stable orbits have been studied, for configuration rotating around such black holes. Static uncharged black hole in general relativity is described by well known and well studied Schwarzschild solution.

However even for large mass black hole (compared to Planck mass) the Schwarzschild solution is a good approximation to describe uncharged black hole in string theory except for regions near the singularity. This situation is completely different for the Einstein-Maxwell solution in string inspired theory due to dilaton coupling.

The dilaton couples with F^2 with implication that every solution having non zero $F_{\mu\nu}$ couples with dilaton. Thus the charged black hole solution in general relativity (the Reissner-Nordström solution) appears in string theory with presence of dilaton. Thus the effective four dimensional low energy action is given by,

$$S = \int d^4x\sqrt{-g}\left[-R + e^{-2\Phi}F^2 + 2(\nabla\Phi)^2\right] \tag{60}$$

where $F_{\mu\nu}$ is the Maxwell field and we have set other gauge and antisymmetric tensor field, e.g. the Kalb-Ramond field $H_{\mu\nu\rho}$ to zero in order to focus on dilaton field Φ [27, 28, 29, 30, 65]. Extremizing the above action with respect to the $U(1)$ potential A_μ, dilaton field Φ and metric $g_{\mu\nu}$ lead to the following field equations,

$$\nabla_\mu\left(e^{-2\Phi}F^{\mu\nu}\right) = 0 \tag{61}$$

$$\nabla^2\Phi + \frac{1}{2}e^{-2\Phi}F^2 = 0 \tag{62}$$

$$R_{\mu\nu} = 2\nabla_\mu\Phi\nabla_\nu\Phi + 2e^{-2\Phi}F_{\mu\lambda}F^\lambda_\nu - \frac{1}{2}g_{\mu\nu}e^{-2\Phi}F^2 \tag{63}$$

The static spherically symmetric solution to the above field equations yield the line element as [27]:

$$ds^2 = -(1 - \frac{2M}{r})dt^2 + \frac{1}{(1 - \frac{2M}{r})}dr^2 + r(r - e^{2\Phi_0}\frac{Q^2}{M})d\Omega^2 \tag{64}$$

where, $d\Omega^2 = d\theta^2 + sin^2\theta d\phi^2$. Due to isometry we can confine our motion in the equatorial plane such that, $d\Omega^2 = d\phi^2$ [i.e. $\theta = \pi/2$]. Here Φ_0 gives the asymptotic value of dilaton field and Q represents the black hole charge. This solution is almost identical to the Schwarzschild metric with the difference being that areas of two spheres depend on Q. The surface $r = \frac{Q^2e^{2\Phi_0}}{M}$ is singular and $r = 2M$ is the regular event horizon. The solution of the scalar field Φ as a function of r in terms of its asymptotic value Φ_0 can be obtained from Eq. (62) leading to the following result [27]:

$$e^{-2\Phi} = e^{-2\Phi_0} - \frac{Q^2}{Mr} \tag{65}$$

From the above result note that we have the following limit, $r \to \infty$ leading to $\Phi \to \Phi_0$. Thus the dilaton charge can be defined as,

$$D = \frac{1}{4\pi}\int d^2\sigma^\mu\nabla_\mu\Phi \tag{66}$$

where the integral is over the two sphere located at spatial infinity and σ^μ is the normal to the corresponding two sphere at spatial infinity. For the charged black hole we are considering this leads to,

$$D = -\frac{Q^2e^{2\Phi_0}}{2M} \tag{67}$$

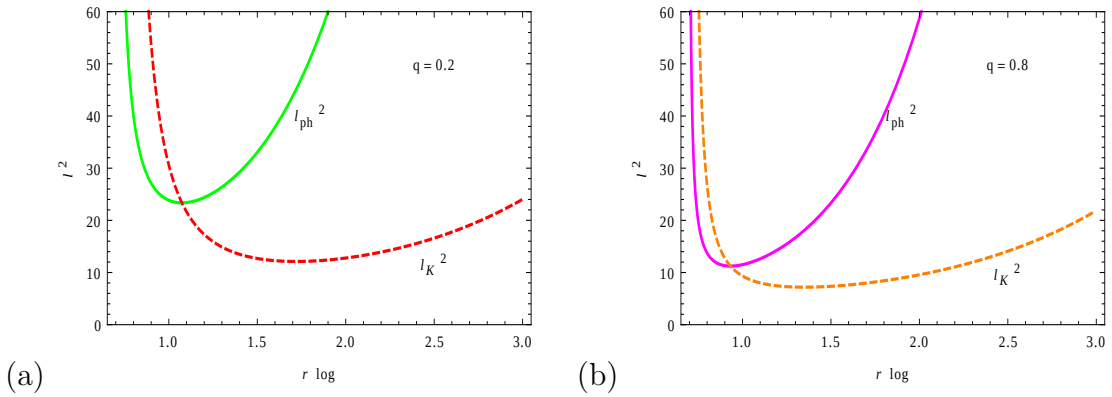

(a) (b)

Figure 3. The figures show the behavior of $l^2_{ph}(r,q)$ and $l^2_K(r,q)$ with radial variable for different values of dilaton charge q. All of them are in the units of M. Here we have all the figures in the range $q < 1$. The curve for $\ell^2_K(r,y)$ has only growing part showing only existence of inner ring. Thus no inner cusp exists in these spacetime.

Note that dilaton charge D depends on the asymptotic value of dilaton field Φ_0, which is determined solely by M and Q and is always negative.

One point must be mentioned while passing, that this charge originates from coupling of electromagnetic field with a scalar field, the actual charge present in the system is the electromagnetic charge Q. If there were no electromagnetic charge the dilaton charge D defined through Eq. (67) would have been zero. Hence this dilaton charge is not a scalar charge it's a coupling between the electromagnetic charge and the scalar field at asymptotic infinity. This charge is also responsible for long range attractive force between black holes [27].

Note that the actual dependence on dilaton field depends on Planck scale described by, $e^{-\Phi/M_{pl}}$. Since we have worked in the unit $M_{pl} \sim 1$ the term modified to $e^{-\Phi}$. As $\Phi \to \Phi_0 \sim M_{pl}$, this term become significant. For notational convenience we shall define a quantity $q = -D$ and by virtue of above discussion q is always positive. Hence our solution is parameterized by the variable q and choosing the dimensionless expression such that $M = 1$ we get the line element as

$$ds^2 = -\left(1 - \frac{2}{r}\right) dt^2 + \left(1 - \frac{2}{r}\right)^{-1} dr^2 + r\,(r-2q)\,d\Omega^2 \tag{68}$$

Then we have two horizons in our system given by $r_{h1} = 2$ and $r_{h2} = 2q$. We shall took the choice in which $r_{h1} > r_{h2}$ or equivalently $q \leq 1$. Thus equilibrium configurations are possible only for $r > 2$. Now the equipotential surfaces are possible only in these spacetimes. Now, the equipotential surfaces are determined by the result,

$$W(r,\theta) = \frac{1}{2} \ln \frac{\left[r(r-2)(r-2q)\sin^2\theta\right]}{\left[r^2(r-2q)\sin^2\theta - (r-2)\ell^2\right]} \tag{69}$$

and

$$\frac{d\theta}{dr} = \frac{r^2(r-2q)^2\sin^2\theta - \ell^2(r-2)^2(r-q)}{\ell^2 r(r-2)^2(r-2q)} \tan\theta \tag{70}$$

For $q = 0$ the above results reduces to the well known Schwarzschild result [37]. The best insight into the nature of the ℓ = constant fluid configurations are obtained by examining the behavior of $W(r, \theta)$ in the equatorial plane ($\theta = \pi/2$). There are two reality conditions on $W(r, \theta = \pi/2)$:

$$r > 2; r > 2q \tag{71}$$

and

$$r^2(r - 2q) > r^2\ell^2 \tag{72}$$

The first condition is just the statement that the fluid should remain outside the black hole horizons and we shall calculate it's property in that non singular region of spacetime. While the second condition implies,

$$\ell^2 \leq \ell^2_{ph}(r; q) \equiv \frac{r^2(r - 2q)}{r^2} \tag{73}$$

This function $\ell^2_{ph}(r; q)$ can be thought of as an effective potential of the photon geodesic motion, also note that $\ell = \frac{U_\phi}{U_t}$ has a close correspondence with the impact parameter for photon geodesic motion [57]. Further the condition to obtain local extrema of the potential $W(r, \theta = \pi/2)$ is identical to the condition for vanishing of pressure gradient ($\partial U_t/\partial r = 0, \partial U_t/\partial\theta = 0$). Since at the equatorial plane we have $\partial U_t/\partial\theta = 0$ independently along with the criteria ℓ = constant, and the following relation:

$$\frac{\partial U_t}{\partial r} = \frac{r^2(r - 2q)^2 - \ell^2(r - 2)^2(r - q)}{[r^2(r - 2q) - \ell^2(r - 2)]^{3/2}\,[r(r - 2)(r - 2q)]^{1/2}} \tag{74}$$

From which we arrive at the particular expression for angular momentum density,

$$\ell^2 = \ell^2_K(r; q) \equiv \frac{r^2(r - 2q)^2}{(r - q)(r - 2)^2} \tag{75}$$

The extrema for $W(r, \theta = \pi/2)$ correspond to the spacetime points, where fluid moves along a circular geodesics, since $\ell^2_K(r; q)$ relates to the distribution of the angular momentum density of circular geodesic orbits. Clearly this leads to,

$$W_{extr}(r, \theta = \pi/2; q) = \ln E_c(r, y) \tag{76}$$

where

$$E_c(r, q) = \frac{(r - 2)\sqrt{(r - q)}}{\sqrt{r}\sqrt{(r - q)(r - 2) - (r - 2q)}} \tag{77}$$

is defined as the specific energy along these circular geodesics. Important properties of the potential $W(r, \theta)$ are determined by its behavior at the equatorial plane, and, specially by the properties of the functions $\ell^2_{ph}(r; q)$ and $\ell^2_K(r, q)$. Discussion of these properties enable us to classify the Dilaton gravity spacetime according to the properties of equipotential surfaces of test particle fluid. For pure Schwarzschild spacetime ($q = 0$) the analysis can be found in Ref. [35].

From the analytical form of $\ell^2_{ph}(r, q)$ it is evident that the quantity diverges at the black hole horizon ($r = 2$). However it shows no such divergence for the inner horizon

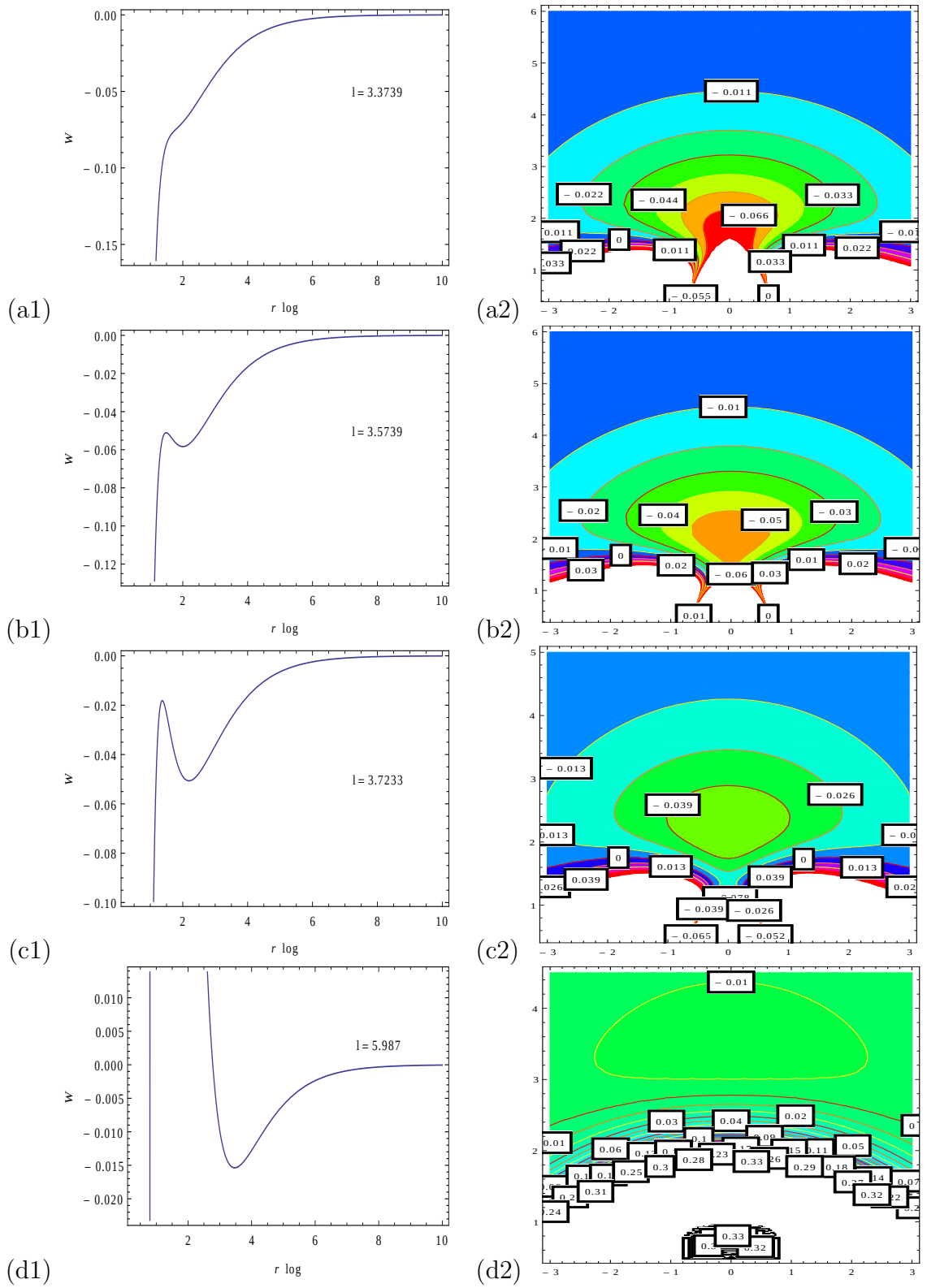

Figure 4. The figures (a)-(d) show the variation of potential $W(r, \theta = \pi/2, q)$ with $log\ r$ in the '1' part and the contour plot of W with $log(r\ \sin\theta)$ and $log(r\ \cos\theta)$ in the '2' part. Each figures are for values of dilaton charge $q < 1$. Here only central rings exists, while no inner cusp comes into existence.

given by $r = 2q$. The local minimum of the function $\ell^2_{ph}(r, q)$ corresponds to the radius of photon circular orbit and has the following expression,

$$r_{ph} = \frac{3 + q \pm \sqrt{(q+3)^2 - 16q}}{2} \tag{78}$$

with the impact parameter,

$$\ell^2_{ph(c)} = \ell^2_{ph(min)} \equiv r^2(r - q) \tag{79}$$

The function $\ell^2_K(r, q)$, determining the Keplerian (geodesic) circular orbits, has a zero point at the so called static radius given by,

$$r_s = 2q \tag{80}$$

which coincides with the inner horizon, also note that the function has divergent nature at $r = 2$ and as well as at $r = q$. The function $\ell^2_K(r; q)$ diverges at the black hole horizon i.e. $\ell^2_K(r \to 2) \to +\infty$. Since,

$$\begin{aligned} \frac{\partial \ell^2_K}{\partial r} &= \frac{4r(r-2q)}{(r-2)^2} \\ &- \frac{r^2(r-2q)^2(3r-2-2q)}{(r-q)^2(r-2)^3} \end{aligned} \tag{81}$$

the local extrema of $\ell^2_K(r, q)$ are given by the condition, $q_{ms} = 1$ determining the marginally stable circular orbits. For $q < q_{ms}$, there exists an inner (outer) marginally stable circular geodesic at $r_{ms(i)}$ $(r_{ms(o)})$.

Other special values of q corresponds to the situation where the value of the minimum of $\ell^2_{ph}(r, q)$ equals the maximum of $\ell^2_K(r, q)$. We denote this value by q_e and is a solution of the algebraic equation,

$$q_e^5 - 22q_e^4 + 80q_e^3 - 64q_e^2 - 32 = 0 \tag{82}$$

However this situation is less important as the above equation has no physical solution. Thus we will not have any inner cusp present in the system. Hence this has less attractive features, still interesting which we will present now.

In this situation the behavior of ℓ^2_{ph} and ℓ^2_K are similar to that of RN scenario. while we have only four available situations. As illustrated in Fig. 3 we have a minimum for ℓ^2_K having value, $\ell_{ms} = 3.5739$. We also have a minimum in ℓ^2_{ph} which corresponds to the value, $\ell_{ph(c)} = 4.2786$. Thus all together we have four cases in this dilaton gravity model from behavior of the potential $W(r, \theta = \pi/2, q)$. These cases are given for following intervals of ℓ:

(i) $\ell < \ell_{ms}$. We have only open equipotential surfaces in this angular momentum range [see Fig. 4a1-2].

(ii) $\ell = \ell_{ms}$. An infinitesimally thin and unstable rings comes to existence at the marginally stable radius [see Fig. 4b1-2].

(iii) $\ell_{ms} < \ell \leq \ell_{ph(c)}$. Closed equipotential surfaces comes into existence, with one such surface having cusp, allowing inflow to the black hole [see Fig. 4c1-2]

(iv) $\ell > \ell_{ph(c)}$. Closed equipotential surfaces exist, however cusps does not exist. Thus in the near horizon region equipotential surfaces cannot cross equatorial plane [see Fig. 4d1-2].

Thus we have obtained structure of equipotential surfaces in dilaton gravity. How the inflow occur in this spacetime along with necessary criteria on the angular momentum density. Also behavior in determining the angular momentum density which admits no minima. Hence this can be thought of having less structure than the previous one still having quiet interesting features.

4.4. Einstein-Maxwell-Gauss-Bonnet Gravity

In high energy physics, assuming spacetime to have more than four dimensions is a common practice. In these scenarios, the spacetime is assumed to be a four dimensional brane, embedded on a higher dimensional bulk. Though ordinary matter fields are confined to these branes, gravity can interact via bulk as well. The EH action needs to be modified as well and the most natural choice would be to include higher order terms in the action. A famous second order term is called the Gauss Bonnet term, under whose presence the modified action looks like,

$$S = \int dx^5 \sqrt{-g}\Big[R + \alpha\Big(R_{abcd}R^{abcd} - 4R_{ab}R^{ab} + R^2\Big) + F_{ab}F^{ab}\Big] \tag{83}$$

where R, R_{ab} and R_{abcd} are Ricci scalar, Ricci tensor and Riemann tensor respectively. F_{ab} is the electromagnetic tensor field and α being the GB coupling coefficient with dimension of length squared. In order to get equations of motion we need to vary the action with respect to the metric g_{ab} and electromagnetic field F_{ab} respectively. This leads to [66],

$$\begin{aligned} R_{ab} \quad & - \frac{1}{2}g_{ab}R - \alpha\Big[\frac{1}{2}g_{ab}\Big(R_{pqrs}R^{pqrs} \\ & - 4R_{mn}R^{mn} + R^2\Big) - 2RR_{ab} + 4R_{am}R^{m}_{b} \\ & + 4R^{mn}R_{ambn} - 2R_{a}^{\ pqr}R_{bpqr}\Big] = T_{ab} \end{aligned} \tag{84}$$

$$\nabla_a F^{ab} = 0 \tag{85}$$

where T_{ab} is the usual stress tensor for electromagnetic field. The important thing to notice is that the field equation only contains second order derivatives of the metric, no higher derivatives are present. This is expected since Gauss-Bonnet gravity is a subclass of Lovelock gravity, which does not contain higher derivative terms of the Riemann tensor.

Now it is possible to obtain static spherically symmetric solution to this field equation having the form of Eq. (11). It turns out that those solutions are asymptotically de Sitter or anti-de Sitter. Thus this situation would be identical to that in Sec. 4.2. This immediately tells us that only a correspondence between the parameters in this theory have to match with that of charged $F(R)$ scenario discussed in an earlier section.

To this end we must mention that the solution obtained above corresponds to a five-dimensional spacetime, i.e. the line element takes the form: $ds^2 = -f(r)dt^2 + f^{-1}(r)dr^2 + r^2 d\Omega_3^2$, where $d\Omega_3^2 = d\theta_1^2 + \sin^2\theta_1(d\theta_2^2 + \sin^2\theta_2 d\theta_3^2)$. However as we have been emphasizing that this solution can be interpreted from a brane world point of view, such that the visible brane is characterized by $\theta_3 =$ constant hypersurface. Hence the solution reduces to four dimension with $(t, r, \theta_1, \theta_2)$ as a set of coordinates. Thus on the visible brane the spherically symmetric solution can be treated at the same footing to those discussed earlier. Such spherically symmetric solutions are obtained in Ref. [66] and has the particular form with reference to Eq. (11) as

$$f(r) = K + \frac{r^2}{4\alpha}\left[1 \pm \sqrt{1 + \frac{8\alpha\,(m + 2\alpha \mid K \mid)}{r^4} - \frac{8\alpha q^2}{3r^6}}\right] \tag{86}$$

where K determines the scalar curvature of the spacetime, to which we attribute a positive value. Then form solar system tests and neutrino oscillation experiments [67, 68] it turns out that α^{-1} has stringent bounds. Also in all astrophysical scenarios the distance from black hole r is quiet large, thus for our study we can make a power series expansion of the terms inside the square root and arrive at the following form:

$$f(r) = 1 + \frac{r^2}{2\alpha} + \frac{m + 2\alpha}{r^2} - \frac{q^2}{3r^4} \tag{87}$$

Then we readily identify this with Eq. (44) leading to the following mapping, $\alpha = -1/(2y)$. The possibility that α may be negative has been discussed in detail by [69] and [70]. With this identification we can run all our machinery described in previous sections and obtain all the relevant physical quantities.

All the numerical values for cosmological parameter discussed earlier is directly mapped to that of α. We can also conclude that it has identical structure of equipotential surfaces, with existence of inner and outer cusp. Thus matter outflow can also occur in this topological dS or AdS black holes along with possibility of inflow to it.

Some numerical estimates can be made for this model following previous discussions. The angular momentum density for inner and outer marginally stable orbits are, 3.04 and 4.9 respectively with $\alpha = 5 \times 10^5$. Also marginally bound and photon circular orbits have similar expressions.

Thus for various alternative gravity theories we have obtained the equipotential surfaces for rotating perfect fluid. For some of them we have observed dynamical accretion disk requiring inflow, outflow and cusps. While in some cases the structure was simpler and do not have such dynamical behaviour. Thus we may conclude that black holes in different alternative theories affect accretion disk structure differently.

5. Conclusions

The effect of additional higher curvature correction terms in the EH action on the structure of equipotential surfaces for perfect fluid rotating around black holes in these modified gravity theories have been investigated. For that purpose we have performed

the whole analysis for an arbitrary static spherically symmetric spacetime. Then we have applied the results obtained to different classes of alternative theories, with higher curvature terms. These theories include: charged $F(R)$ theory, dilaton induced gravity theory and finally the Einstein-Maxwell-Gauss-Bonnet gravity. In the $F(R)$ theory and EMGB theory the black hole solutions asymptotically behave as dS or AdS. The equilibrium structure of perfect fluid orbiting around these black holes in the above mentioned alternative gravity theories lead to modifications of the equipotential contours. Having provided the basic features let us now summarize the results:

- For the situation, $\ell = 0$, we always have an open equipotential surface. The potential is being determined by the relation, $W = \ln\sqrt{f(r)}$. Thus different spherically symmetric solution leads to different equipotential surfaces.
- Existence of outer cusp does not facilitate accretion onto the black hole. We need to have inner cusp for the equipotential surfaces as well, in order to have inflow to the black hole. Note that outer cusp is also necessary for accretion to occur.
- Closed equipotential surfaces are possible if and only if the angular momentum lies in the range, $\ell \in \left(\ell_{ms(i)}, \ell_{ms(o)}\right)$. The quantities, $\ell_{ms(i)}$ and $\ell_{ms(o)}$ represents the local minima and maxima of the angular momentum density respectively. For the charged $F(R)$ theory closed surfaces comes into existence provided the cosmological parameter y satisfies, $y < y_{ms} = 0.000692$. While for the EMGB gravity we obtain, $\alpha_{ms} = -782.47$. Note that these closed surfaces are necessary for existence of toroidal accretion disc.
- The accretion by Paczyński mechanism becomes possible, if angular momentum density lies in the range, $\ell \in \left(\ell_{ms(i)}, \ell_{mb}\right)$, where ℓ_{mb} being the corresponding value of angular momentum density for marginally bound circular geodesics. In this scenario, the outflow from accretion disc becomes possible through both the inner and outer cusps. The existence of inner cusp leads to accretion flow directed towards the black hole.
- For marginally stable configurations, due to overfilling of marginally closed equipotential surfaces efficient inflow and outflow occurs. However very near the horizon, the behaviour may change significantly.
- Another physical situation of interest corresponds to the angular momentum range: $\ell \in \left(\ell_{mb}, \ell_{ms(o)}\right)$. In this situation the flow down to the black hole becomes non-existent since open self-crossing surfaces come into existence.
- Finally, for the situation where, $\ell > \ell_{ms(o)}$, the toroidal structure cannot exist. Equipotential surfaces exist however they are always open. Also the surfaces becomes narrower as it approaches the static radius which may have a significant effect on collimation of jets from the black hole.

These effects were most prominent for accretion of perfect fluid to the black holes in $F(R)$ theory and the EMGB theory. Both of which are asymptotically de Sitter for certain choice of parameter space. Richness in the structure of black hole accretion disk

for asymptotically de Sitter solutions in GR were pointed out earlier in [48]. Thus it is evident from this work that their generalization to alternative theories also come up with varied structure of the accretion disk. There are also asymptotically flat solutions like the dilaton black hole, which have new features compared to the GR scenario. However in this spacetime accretion disk does not posses all the structures which were present in the other two cases.

Thus we observe that in Einstein gravity as well as in alternative theories spacetime with analogue of repulsive cosmological constant (for instance, y in $F(R)$ model, $1/\alpha$ in EMGB theory) shows wide variety of phenomenon as the accretion disk structure is considered. Though the structure of the accretion disk changes considerably due to presence of higher curvature correction terms in the EH action it is very difficult to detect their signature astrophysically. This is mainly due to the reason that the parameter space of these alternative theories for being of astrophysical interest is quiet large compared to present day estimates of those parameters. For example, the black holes fuelling active galactic nuclei have typical masses in the range, $\sim 10^8 M_\odot - 10^9 M_\odot$ which leads to an estimation of the cosmological parameter as, $y < 10^{-10}$, which is very small and thus will not result in significant changes in the accretion disk structure.

However the primordial black holes have a much larger value of the cosmological parameter. Thus accretion structure of them could be best hope to test these alternative theories. However this is beyond the scope of present day observations. Even though the departure of the equipotential contours in alternative theories from their general relativistic counterpart due to presence of higher curvature correction terms is an important effect but is unlikely to be observed in near future.

To summarize, in this work we have discussed various possible candidates for alternative theories and the accretion disk structure in them. We have also left some questions unanswered. Among them the runaway instability criteria for toroidal accretion disks, i.e. stability with time has not been addressed as well as the self-gravitation influence of the disk is also not considered. These we leave for future.

Acknowledgement

The author is funded by a SPM fellowship from CSIR, Govt. of India. The author would also like to thank Prof. T. Padmanabhan, Prof. Subenoy Chakraborty and Suprit Singh for helpful discussions. He also likes to thank the referees for providing valuable comments that have helped to improve the manuscript.

References

[1] M. Kramer, *Int. J. Mod. Phys. D* **23**, 1430004 (2014).
[2] M. Kramer and I.H. Stairs, *Annu. Rev. Astron. Astrophys.* **46** 541 (2008).
[3] M. Kramer and N. Wex, *Class. Quant. Grav.* **26**, 073001 (2009).
[4] B.M. Peterson, *An introduction to active galactic nuclei*, Cambridge University Press, Cambridge (1997).

[5] D.E. Osterbrock, *Rep. Prog. Phys.* **54**, 579 (1991).
[6] A.G. Riess et. al., *Astron. J.* **116**, 1009 (1998).
[7] S. Perlmutter et. al., *Astrophys. J.* **517**, 565 (1999).
[8] S. Nojiri and S.D. Odinstov, *Phys. Lett. B* **652**, 343 (2007); *ibid* **657**, 238 (2007).
[9] A. D. Felice and S. Tsujikawa, *Living Rev. Relativity* **13**, 3 (2010).
[10] V. Faraoni, *Phys. Rev. D* **75**, 067302 (2007) arXiv:gr-qc/0703044.
[11] S. Nojiri and S.D. Odinstov, *Phys. Rept.* **505** 59 (2011).
[12] I.L. Buchbinder, S.D. Odinstov and I.L. Shapiro, (1992) *Effective Action in Quantum Gravity*, IOP Publishing, Bristol.
[13] D.V. Vassilevich, *Phys. Rept.* **388**, 279 (2003).
[14] C. Lanczos, *Z.Phys.* **73**, 147 (1932);
C. Lanczos, *Ann. of Math.* **39**, 842 (1938).
[15] D. Lovelock, *J. Math. Phys.* **12**, 498 (1971).
[16] T. Padmanabhan, *Gravitation: Foundation and Frontiers*, Cambridge University Press, Cambridge, UK (2010).
[17] T. Padmanabhan and D. Kothawala, *Phys. Rept.* **531**, 115 (2013).
[18] T. Padmanabhan, *Phys. Rev. D* **84**, 124041 (2011) arXiv:1109.3846.
[19] K. Bamba K. and S.D. Odinstov, *JCAP* **0804**, 024 (2008);
S.M. Carroll, V. Duvvuri, M. Trodden and M.S. Turner, *Phys. Rev. D* **70**, 043528 (2004).
[20] A.A. Starobinsky, *Phys. Lett. B* **91**, 99 (1980).
[21] M.C.B. Abdalla, S. Nojiri and S.D. Odinstov, *Class. Quant. Grav.* **22**, L35 (2005);
S. Nojiri and S.D. Odinstov, *Phys. Rev. D* **78**, 046006 (2008).
[22] C. Corda, *Eur. Phys. J. C* **65**, 257 (2010);
C. Corda, *Int. J. Mod. Phys. D* **18**, 2275 (2009).
[23] M. Takada and B. Jain, *Mon. Not. Roy. Astron. Soc.* **348**, 897 (2004).
[24] R.P. Woodard, *Lect. Notes Phys.* **720**, 403 (2007).
[25] S. Chakraborty and S. SenGupta, *Phys. Rev. D* **90**, 047901 (2014) arXiv:1403.3164.
[26] D.G. Boulware and S. Deser, *Phys. Rev. Lett.* **55**, 2656 (1985).
[27] D. Garfinkle, G.T. Horowitz and A. Strominger, *Phys. Rev. D* **43**, 3140 (1991).
[28] S. Coleman, in *The Unity of the Fundamental Interactions*, edited by A. Zichichi (Plenum, London) (1983).
[29] H.J. De Vega and N. Sanchez, *Nucl. phys. B* **309**, 552 (1988).
[30] E. Witten, (ed.) *Gravitation: An Introduction to Current Reaserch*, (Wiley, N.Y.) (1962).
[31] M.A. Abramowicz and M.J. Percival, *Class. Quanta. Grav.* **14**, 2003 (1997).
[32] I.F. Mirabel and L.F. Rodríguez, *Annu. Rev. Astron. Astrophys.* **37**, 409 (1999).
[33] R.P. Fender, M.M. Hanson and G.G. Pooley, *Mon. Not. Roy. Astron. Soc.* **308**, 473 (1999).
[34] I.D. Novikov and K.S. Thorne, In: C. DeWitt and B.S. DeWitt (eds.) *Black Holes*, Gordon and Breach, N.Y. (1973).
[35] M. Kozlowski, M.Jaroszyński and M.A. Abramowicz, *Astron. and Astrophys.* **63**, 209 (1978).
[36] M.A. Abramowicz, M. Jaroszyński and M. Sikora, *Astron. Astrophys.* **63**, 221 (1978).
[37] M. Jaroszyński, M.A. Abramowicz and B. Paczyński, *Acta Astron.* **30**, 1 (1980).
[38] D. Lynden-Bell, *Nature* **223**, 690 (1969).
[39] R.D. Blandford, In: S.W. Hawking, W. Israel(eds.) *Three hundred years of gravitation*, Cambridge University Press, Cambridge, p.277 (1987).
[40] J. Antoniadis et. al. *Science*, **340**, 448 (2013).
[41] P.C.C. Freire et. al. *Mon. Not. R. Acad. Sci.* **423**, 3328 (2012).
[42] D.N. Spergel et. al., *Astrophys. J. Suppl.* **148**, 175 (2003).
[43] D.N. Spergel et. al., *Astrophys. J. Suppl.* **170**, 377 (2007).
[44] O. Shemmer, H. Netzer, R. Maiolino, E. Oliva, S. Croom, E. Corbett and L. di Fabrizio, *Astrophys. J.* **614**, 547 (2004).
[45] Z. Stuchlík, *Mod. Phys. Lett. A* **20**, 561 (2005).

[46] R.H. Boyer, *Proc. Cambridge Phil Soc.* **61**, 527 (1965).
[47] M.A. Abramowicz, *Acta Astron.* **24**, 45 (1974).
[48] Z. Stuchlík, P. Slaný and S. Hledík, *Astron. Astrophys.* **363**, 425 (2000).
[49] Z. Stuchlík, P. Slaný, and J. Kováî, *Class. Quant. Grav.* **26**, 215013 (2009).
[50] L.G. Fishbone, V. Moncrief, *Astrophys. J.* **207**, 962 (1976).
[51] L.G. Fishbone, *Astrophys. J.* **205**, 323 (1977).
[52] B. Paczyński and P. Witta, *Astron. and Astrophys.* **88**, 23 (1980).
[53] M.A. Abramowicz, M. Calvani and L. Nobili, *Astrophys. J.* **242**, 772 (1980).
[54] S. Chakraborty and S. Chakraborty, *Can. J. Phys.* **85**, 689 (2011) arXiv:1109.0676.
[55] S. Chakraborty, *Astrophys. Space Sci.* **347**, 411 (2013) arXiv:1210.1569.
[56] F.H. Seguin, *Astrophys. J.* **197**, 745 (1975).
[57] Z. Stuchlík and S. Hledík, *Phys. Rev. D* **60**, 044006 (1999).
[58] J. Kovár, P. Slaný, C. Cremaschini, Z. Stuchlík, V. Karas and A. Trova, *Phys. Rev. D* **90**, 044029 (2014).
[59] P. Slaný, J. Kovár, Z. Stuchlík and V. Karas, *Astrophy. J. Suppl.* **205**, 3 (2013).
[60] R.E. Smith et al., *Mon. Not. Roy. Astron. Soc.* **341**, 1311 (2003).
[61] S.H. Hendi, B.E. Panah and S.M. Mousavi, *Gen. Relt. Grav.* **44**, 835 (2012).
[62] G. Cognola, F. Elizalde, S. Nojiri, S.D. Odinstov, L. Sebastiani and S. Zerbini, *Phys. Rev. D* **77**, 046009 (2008).
[63] P. Zhang, *Phys. Rev. D* **76**, 024007 (2007).
[64] M. Capone and M.L. Ruggiero (2009) arXiv:0910.0434.
[65] J. Bekenstein, *Phys. Rev. D* **5**, 1239 (1972); *ibid*, *Ann.phys.* (N.Y.) **91**, 75 (1975); N. Bocharova, K. Broonikov and V. Melnikov, *Vestn.Mosk.Univ.Fiz.Astron.* **6**, 706 (1970).
[66] M.H. Dehghani, *Phys. Rev. D* **70**, 064019 (2004).
[67] S. Chakraborty and S. SenGupta, *Phys. Rev. D* **89**, 026003 (2014) arXiv:1208.1433.
[68] S. Chakraborty, *Class. Quanta. Grav.* **31**, 055005 (2014) arXiv:1309.0693.
[69] M.H. Dehghani, *Phys. Rev. D* **70**, 064009 (2004) arXiv:hep-th/0404118.
[70] O. Corradini, *Mod. Phys. Lett. A* **20**, 2775 (2005) arXiv:hep-th/0405038.